

On performance analysis of non-orthogonal multiple access downlink for cellular-connected unmanned aerial vehicle relaying assisted vehicle-to-everything system

Hong-Nhu Nguyen¹, Nhat-Tien Nguyen¹, Gia-Thinh Vo²

¹Faculty of Electronics and Telecommunications, Saigon University, Ho Chi Minh City, Vietnam

²Institute of Engineering-Technology, Thu Dau Mot University, Binh Duong, Vietnam

Article Info

Article history:

Received Sep 7, 2023

Revised Nov 2, 2023

Accepted Nov 4, 2023

Keywords:

Decode-and-forward

Relays

Power beacon

Non-orthogonal multiple access throughput

Wireless energy harvesting multi-hop

ABSTRACT

This paper presents the unmanned aerial vehicle (UAV) relays' assisted vehicle-to-everything (V2X) network to implement the internet of things (IoT) systems with improvement in the coverage area. Such a network benefits from many advantages of the non-orthogonal multiple access (NOMA) scheme. We have implemented a decode-and-forward (DF) scheme for these UAVs. Then, we characterize the channels as Nakagami-m fading to evaluate the performance of the system. We derive closed-form expressions of outage probability (OP), ergodic capacity (EC), and throughput. The results show that the performance of the system depends on the transmitted signal-to-noise ratio (SNR) at the base station and the heights of the UAV relays. Target rate and power allocation factors are two main parameters that can be adjusted to achieve better performance. The results also compare to the system without UAV and OMA technique that shows the advantages of deploying UAV-assisted NOMA. Therefore, the design of NOMA for UAV relay-assisted V2X systems provides sufficient demand. The simulation results verified the effectiveness of the proposed UAV network and the precision of the theoretical analysis.

This is an open access article under the [CC BY-SA](https://creativecommons.org/licenses/by-sa/4.0/) license.



Corresponding Author:

Gia-Thinh Vo

Institute of Engineering-Technology, Thu Dau Mot University

Binh Duong Province, Vietnam

Email: thinhvg@tdmu.edu.vn

1. INTRODUCTION

In recent years, global demand for unmanned aerial vehicles (UAVs) or drones has increased due to their capability and cost effectiveness. UAV networks benefit from various applications with complex duties, for instance, traffic monitoring, aerial imaging, cargo transport, and communication platform [1]. It is really necessary to implement high-performance UAV ground networks to shift the way towards the forthcoming approach of "internet of drones" [2]. In particular, low latency, ubiquitous coverage, and high reliability throughput are the main benefits of UAV-based networks that perform real-time control and command for UAV safety operation as well as payload data communication targeted to users at ground [3]. In most UAV networks, the simple direct point-to-point transmissions using the unlicensed spectrum (i.e., scientific, industrial and medical (ISM) bands) are deployed to allow UAVs to communicate with the ground users. Such UAV networks have limitations that are unreliable, insecure, vulnerable to interference, and low data rate. In specific situations, applications of UAVs in the future are limited due to their operation within the visual line-of-sight (VLoS) constraint. Recently, UAVs have been combined with the cellular network as new aerial user equipment (UEs) to form cellular-connected UAVs, which have been recognized as a promising approach.

More specifically, cellular-connected UAVs are expected to exhibit significant performance improvement in terms of coverage, reliability, and throughput compared to point-to-point UAV ground networks developed in the literature [4]. An interest base station (BS) cooperative beamforming (CB) approach was developed for the cellular downlink to eliminate the strong interference caused by the co-channel terrestrial transmissions associated with a particular UAV [5]. To effectively suppress terrestrial interference, the BSs' serving of the UAV employs a CB-based interference transmission paradigm [5]. Mei *et al.* [6] studied the uplink transmission of BSs to UAV enabling spectrum sharing with existing ground users. The optimal inter-cell interference coordination (ICIC) architecture and air-ground performance trade-off are introduced to achieve the optimal weighted sum-rate of the UAV and existing ground users. In particular, they jointly optimized the UAV's uplink cell associations and power allocations over multiple resource blocks to achieve such optimization.

UAV-based networks provide greater wireless coverage in both rural and urban areas [7]. Therefore, the performance of UAV networks can be significantly improved in various scenarios and approaches in recent research advances [8]–[16]. For example, to maximize network throughput, Zeng *et al.* [8] considered the UAV that acts as a mobile relay by optimizing the transmit power and trajectory of the UAV relay. The secure transmission problem can be addressed with physical layer security (PLS)-assisted UAV network [9]. They considered the problem of maximization of the secrecy rate by optimizing the source/relay transmission power [9]. Fan *et al.* [10] studied the approach to achieve optimal network throughput in a UAV relaying network, i.e., they jointly optimized bandwidth, rate, transmit power and location of the UAV. The authors in [11] developed a hybrid satellite-terrestrial network, in which a satellite communicates with a ground user equipment (UE) by enabling multiple decode-and-forward (DF) three-dimensional (3-D) mobile UAV relays. Mamaghani and Hong [12] presented a cooperative secure UAV-assisted transmission mechanism, where a source benefits from an energy-constrained UAV-mounted amplify-and-forward relay to forward confidential signals to a destination in the presence of a ground eavesdropper [14]–[16].

Unlike conventional cellular communication, design of multi-antenna array transmission with spatial diversity allows systems to suffer a rich scattering environment; a single-antenna UAV exhibits much poorer scattering in downlink communication. It is not efficient if multiple users need to share the communication bandwidth of the same UAV at the same time. Meanwhile, non-orthogonal multiple access (NOMA) is introduced to simultaneously serve multiple users without orthogonal resources. To expand service coverage, NOMA can be integrated with cooperative networks [17], [18], to form cooperative NOMA. In such a cooperative NOMA, transmit signals are separated in the power domain to serve many users [19]–[21]. Far users receive a lower received signal power, whereas near users are allocated a higher signal power. As a result, NOMA can improve the far users' rates once the near users are able to access the transmit signals intended for the far users [21], [22]. The work in [22] studied fixed power allocation and performance degradation is predicted in worse situations, in which the non-optimal power approach and the imperfect channel state information (CSI) occur. The authors addressed the interesting mechanism to serve multi-pair of users. In particular, in which a group of users can communicate with other users to achieve acceptable throughput, which is evaluated by two metrics, that is, the delay-limited mode and throughput delay-tolerant mode.

To analyze the system performance of UAV-enabled systems, some recent studies have presented the UAV network in the context of NOMA [23]–[25]. Mei and Zhang [23] considered a UAV-enabled system to mitigate the UAV's uplink interference without significantly compromising its achievable rate, and such a model benefits from existing backhaul links between BSs. In particular, some BSs are selected to decode the UAV's signals first and retransmit the decoded signals to the backhaul-connected BSs. Hu *et al.* [24] characterized globally optimal solutions by joint optimization problems of UAV position and power allocation. In other promising systems, vehicle-to-everything (V2X) communications are studied through various applications related to vehicles, passengers and pedestrians, vehicle traffic, and drivers. Therefore, V2X systems benefit our future daily life in terms of a safer and more efficient driving experience. As a requirement, critical safety services supported by V2X communications are required to achieve low latency and high-reliability (LLHR) [26]. Specifically, delay-sensitive services will achieve end-to-end latency of a few milliseconds [27]. Inspired by the above observations, the literature introduced combining NOMA into 5G V2X communications to investigate the power allocation problem for both broadcast and multicast cases. For example, Abbasi *et al.* [28] studied trajectory planning and power allocation for a V2X in which an unmanned aerial vehicle (UAV) is considered as a relay to extend coverage for two disconnected far vehicles. They claimed that in a two-user network with an amplify-and-forward (AF) relay, NOMA always has better or equal sum-rate in comparison to orthogonal-multiple-access (OMA) at high signal-to-noise-ratio (SNR) regime. Zhang *et al.* [29] explored ultra-reliable and low latency communications (URLLC) in V2X communications by enabling a full duplex NOMA (FD-NOMA) for their system model. From above discussion of related works and rapid development of cellular networks, performance evaluation of cellular

V2X networks takes advantage of NOMA and forwarding techniques under specific channel conditions applying to mobile network models such as Nakagami-m is a still potential and necessary research area.

The big problem of ensuring safety in V2X requires that the quality of the connection from the vehicle to the server must be maintained constant during the movement of vehicles, which can be interrupted by obstacles such as buildings, trees, and traffic vehicles. To the best of the authors' knowledge, this important aspect has been addressed by integrating UAV in existing V2X systems. In this article, we consider the ground-aerial downlink NOMA cellular networks which consists of a UAV and multiple vehicles. Specifically, the NOMA downlink protocol is invoked in specific groups of vehicles to target separated quality of service (QoS). Meanwhile, vehicle QoS requirements must be satisfied during the operating time of UAVs, which is designed to improve vehicle performance in cell-edge areas. The main contributions of this paper are as follows.

- We propose a system model using UAVs forward NOMA signals to vehicles to improve the performance of obscured vehicles or distant vehicles.
- We design several groups of vehicles that are served simultaneously by enabling the NOMA scheme. We evaluated two important metrics such as OP, EC and throughput. We mathematically prove that the system performance depends on the strength of the transmit signal at the BS. In particular, the performance of a vehicle can be adjusted by power allocation factors, target rates, and UAVs' locations.
- We provide closed-form expressions of OP based on signal-to-interference-plus-noise ratio (SINR) computed to detect signals. In addition, the formulas for EC and throughput are derived. These metrics correspond to the performance evaluation required for such V2X systems.
- We propose an efficient iterative UAV trajectory design for giving UAV-ground base station (GBS) association order, where the successive convex approximation (SCA) technique is invoked to find a locally optimal solution.
- Numerical results demonstrate that: i) the outage performance of the proposed UAV-NOMA based V2X system can satisfy high quality services in high signal-to-noise ratio (SNR) region of base station; ii) the lower heights of UAVs can improve performance of vehicles; iii) V2X system benefits from NOMA for QoS requirements, which shows superiority compared to the system non using UAV or OMA networks.

Organization: The paper is summarized as follows. Section 2 presents the formulation of SINR, SNR of necessary signal analysis. Section 3 describes OP and EC. Section 4 evaluates the performance of our proposed UAV-NOMA based V2X system using numerical examples. Finally, Section 5 concludes our paper.

2. SYSTEM MODEL

In Figure 1, we study the UAV network containing a base station (BS), in which the system has two UAVs that act as a relay (UA_1, UA_2), and two users following NOMA (V_1, V_2). The key parameters are described in Table 1. In this case, we consider these main nodes in such a UAV network in three-dimensional Cartesian coordinates. In Figure 1, we assume the BS at $(0,0,0)$, then UA_1 and UA_2 are located at $UA_1(0, h_1, r_1)$ and $UA_2(r_2, h_2, 0)$, respectively. Furthermore, we can easily represent the locations of two users (vehicles) V_1 and V_2 at $V_1(0,0, d_1)$ and $V_2(d_2, 0,0)$, respectively.

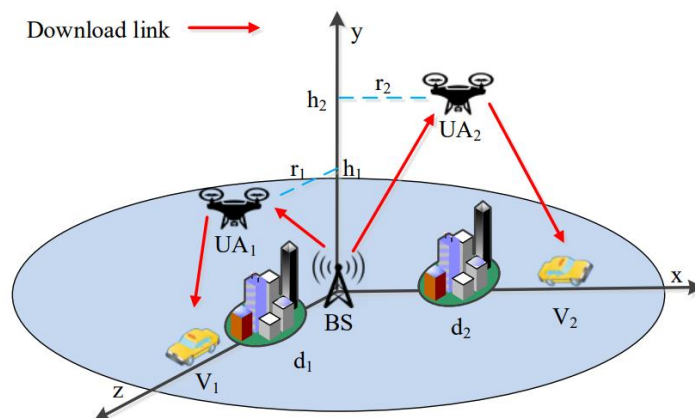


Figure 1. System model for UAV V2X network relying on NOMA

Table 1. Key parameters of the system model

Symbol	Description	Symbol	Description
φ_i	The power allocation coefficient with $i \in \{1,2\}, \varphi_1 + \varphi_2 = 1$ and $\varphi_1 < \varphi_2$	\bar{R}_i	The target rate at V_i
P_S	The transmit power at S	α	The path loss exponent
P_R	The transmit power at $UA_i h_1$	h_1	The channel link between base station and relay UAV UA_1
n_i	The additive white Gaussian noise (AWGN) term followed	h_2	The channel link between base station and relay UAV UA_2
ω_i	The AWGN noise term followed $CN(0, N_0)$	g_1	The channel link between relay UAV UA_1 and V_1
x_i	The information of V_i	g_2	The channel link between relay UAV UA_2 and V_2

The Euclidean distance from BS to $UA_i (i \in \{1,2\})$ and UA_i to V_i , respectively, as (1).

$$d_{BR_i} = \sqrt{r_i^2 + h_i^2}, \text{ and } d_{R_i V_i} = \sqrt{(r_i - d_i)^2 + h_i^2}. \quad (1)$$

Channels $h_i = \frac{\tilde{h}_i}{\sqrt{d_{BR_i}^\alpha}}$ are modeled between the BS and UAVs, and $g_i = \frac{\tilde{g}_i}{\sqrt{d_{R_i V_i}^\alpha}}$ is used as channels between the UAV relays and node V_i , respectively. These channels follow the Nakagami- m distribution.

2.1. Scenario to simulate using UAV

In the first epoch, the BS sends the mixture signal to the two UAV relay nodes UA_1, UA_2 . The signals received at two UAV relays are expressed by (2).

$$y_i = h_i \left(\sqrt{\varphi_1 P_S} x_1 + \sqrt{\varphi_2 P_S} x_2 \right) + n_i, \quad i \in \{1, 2\}, \quad (2)$$

where P_S and P_R are the normalized transmission powers at the BS and the UAV. x_1 and x_2 are the signals for V_1 and V_2 , respectively. The relevant power allocation coefficients are φ_1 and φ_2 . We assume that with to ensure better user fairness. We set n_i the complex Gaussian noise at two UAV relays with $n_i \sim CN(0, N_0)$.

The signal-to-interference-plus-noise ratio (SINR) is used to first detect x_2 at UA_1 is expressed by (3).

$$\Gamma_{R_1, x_2} = \frac{\varphi_2 \rho |h_1|}{\varphi_1 \rho |h_1| + 1}, \quad (3)$$

where $\rho = \frac{P_S}{N_0} = \frac{P_R}{N_0}$ is the transmission SNR at the BS as well as the relays. Keep in mind that x_1 and x_2 should be normalized unity power signals, meaning that $E\{x_1^2\} = E\{x_2^2\} = 1$.

After the success interference cancellation (SIC) happens, SNR is used to detect the signal x_1 at UA_1 :

$$\Gamma_{R_1, x_1} = \varphi_1 \rho |h_1|^2. \quad (4)$$

Similarly, the SNR at UA_2 to detect x_2 is given as (5).

$$\Gamma_{R_2, x_2} = \frac{\varphi_2 \rho |h_2|^2}{\varphi_1 \rho |h_2|^2 + 1}. \quad (5)$$

In the second epoch of communication, each UAV relay UA_i forwards the detected signals to the destinations V_i and the received signal at each user V_i is given as (6).

$$y_{V_i} = \sqrt{P_R} g_i \left(\sqrt{\varphi_1} x_1 + \sqrt{\varphi_2} x_2 \right) + w_i, \quad (6)$$

where w_i are the complex Gaussian noise at V_i with $w_i \sim CN(0, N_0)$. At V_1 , x_2 is decoded first, by treating x_1 as interference, and the received SINR, before and after SIC, are

$$\Gamma_{V_1, x_2} = \frac{\rho \varphi_2 |g_1|^2}{\rho \varphi_1 |g_1|^2 + 1}, \text{ and } \Gamma_{V_1, x_1} = \rho \varphi_1 |g_1|^2. \quad (7)$$

Then, SNR at user V_2 is calculated to detect signal x_2 is given by (8).

$$\Gamma_{V_2, x_2} = \frac{\rho\varphi_2|g_2|^2}{\rho\varphi_1|g_2|^2+1}. \quad (8)$$

2.2. Scenario to simulate without UAV

In this scenario, it is assumed that BS will transfer signals to both users directly rather than using UAV to deliver signals to two users. The received signals at the two cars may then be determined as shown (9).

$$\tilde{y}_{V_i}^{dir} = f_i(\sqrt{P_S\varphi_1}x_1 + \sqrt{P_S\varphi_2}x_2) + \tilde{w}_i^{dir}, i \in \{1,2\}, \quad (9)$$

where \tilde{w}_i^{dir} , i are the complex Gaussian noise at V_i with $w_i \sim CN(0, N_0)$ and $f_i = \frac{\tilde{f}_i}{\sqrt{d_i^\alpha}}$ serves as the channels between the BS and node V_i . These channels follow the Nakagami- m distribution.

In theory, the first user V_1 uses the SIC approach to first decode x_2 and then x_1 . It is necessary to decode these signals using SINR and SNR are.

$$\Gamma_{V_1, x_2}^{dir} = \frac{\varphi_2\rho|f_1|^2}{\varphi_1\rho|f_1|^2+1}, \text{ and } \Gamma_{V_1, x_1}^{dir} = \varphi_1\rho|f_1|^2. \quad (10)$$

Finally, the received SINR at V_2 is computed as (11).

$$\bar{\Gamma}_{V_2, x_2}^{dir} = \frac{\varphi_2\rho|f_2|^2}{\varphi_1\rho|f_2|^2+1}. \quad (11)$$

3. PERFORMANCE ANALYSIS

Considering channel distribution characteristic, let $Z_i = \{|\tilde{h}_i|^2, |\tilde{g}_i|^2\}$ and we have the cumulative distribution function (CDF) and the probability density function (PDF) of Z as [21].

$$F_{Z_i}(x) = 1 - e^{-\Omega_{Z_i}x} \sum_{s=0}^{m_{Z_i}-1} \frac{\Omega_{Z_i}^s x^s}{s!}, \quad (12)$$

where $\Omega_{Z_i} = \frac{m_{Z_i}}{\lambda_{Z_i}}$, m_{Z_i} and λ_{Z_i} are the fading severity parameter and the average power, respectively.

$$f_{Z_i}(x) = \frac{\Omega_{Z_i}^{m_{Z_i}} x^{m_{Z_i}-1} e^{-\Omega_{Z_i}x}}{\Gamma(m_{Z_i})}. \quad (13)$$

Remark 1: Several propagation environments are adopted to analyze the performance and a fading channel model related to the OP of UAV-assisted systems communications in this paper motivated by [30]. We continue to investigate the closed-form expressions for the OP using the Nakagami- m fading model for the mobility of the ground user, which communicates with UAV entities in a realistic propagation environment. We do not compare such fading channels with other models reported in the literature.

3.1. Outage probability of V_1

At destination, V_1 the outage event occurs when either UA_1 or V_1 cannot decode successfully x_1 . Such outage is defined as the probability to SNR less than the pre-defined threshold SNR. We call \bar{R}_1, \bar{R}_2 as target rates for V_1, V_2 then first consider the outage performance of V_1 as (14).

$$\begin{aligned} OP_{V_1} &= 1 - Pr(\Gamma_{R_1, x_2} \geq \varepsilon_2, \Gamma_{R_1, x_1} \geq \varepsilon_1) \times Pr(\Gamma_{V_1, x_2} \geq \varepsilon_2, \Gamma_{V_1, x_1} \geq \varepsilon_1) \\ &= 1 - Pr(|h_1| \geq \chi) Pr(|g_1|^2 \geq \chi), \end{aligned} \quad (14)$$

where, $\varepsilon_1 = 2^{2\bar{R}_1} - 1$, $\varepsilon_2 = 2^{2\bar{R}_2} - 1$ and $\varepsilon_1 = 2^{2\bar{R}_1} - 1\chi = \max\left(\frac{\varepsilon_2}{\rho(\varphi_2 - \varepsilon_2\varphi_1)}, \frac{\varepsilon_1}{\varphi_1\rho}\right)$.

Then, OP_{V_1} is rewritten by (15).

$$\begin{aligned} OP_{V_1} &= 1 - Pr(|h_1|^2 \geq \chi) Pr(|g_1|^2 \geq \chi) = 1 - \bar{F}_{|\tilde{h}_1|^2}(\chi d_{BR_1}^\alpha) \bar{F}_{|\tilde{g}_1|^2}(\chi d_{R_1 V_1}^\alpha) = 1 - \\ &e^{-(\Omega_{\tilde{h}_1} d_{BR_1}^\alpha + \Omega_{\tilde{g}_1} d_{R_1 V_1}^\alpha)\chi} \times \sum_{s=0}^{m_{\tilde{h}_1}-1} \sum_{b=0}^{m_{\tilde{g}_1}-1} \frac{(\Omega_{\tilde{h}_1} d_{BR_1}^\alpha)^s (\Omega_{\tilde{g}_1} d_{R_1 V_1}^\alpha)^b \chi^{s+b}}{s!b!}. \end{aligned} \quad (15)$$

The outage probability of V_1 without UAV is expressed as (16).

$$\begin{aligned} OP_{V_1}^{dir} &= 1 - Pr(\bar{\Gamma}_{V_1, x_2}^{dir} > \varepsilon_2, \bar{\Gamma}_{V_1, x_1}^{dir} > \varepsilon_1) = 1 - Pr\left(|f_1|^2 > \frac{\varepsilon_2}{\rho(\varphi_2 - \varepsilon_2\varphi_1)}, |f_1|^2 > \frac{\varepsilon_1}{\varphi_1\rho}\right) \\ &= 1 - Pr(|f_1|^2 > \chi) = F_{|f_1|^2}(\chi d_1^\alpha). \end{aligned} \tag{16}$$

Using the CDF in (12) we have (17).

$$OP_{V_1}^{dir} = 1 - e^{-\Omega_{\bar{f}_1} d_1^\alpha \chi} \sum_{s=0}^{m_{\bar{f}_1}-1} \frac{(\Omega_{\bar{f}_1} d_1^\alpha)^s \chi^s}{s!} \tag{17}$$

When $\rho \rightarrow \infty$, by using, and hence the $e^{-x} \approx 1 - x$ asymptotic of $OP_{V_2}^\infty$ and $OP_{V_2}^{dir, \infty}$ are given by (18).

$$OP_{V_1}^\infty = 1 - \sum_{s=0}^{m_{\bar{h}_1}-1} \sum_{b=0}^{m_{\bar{g}_1}-1} \frac{\chi^{s+b} (1 - (\Omega_{\bar{h}_1} d_{BR_1}^\alpha + \Omega_{\bar{g}_1} d_{R_1 V_1}^\alpha) \chi)}{s! b! (\Omega_{\bar{h}_1} d_{BR_1}^\alpha)^{-s} (\Omega_{\bar{g}_1} d_{R_1 V_1}^\alpha)^{-b}}, \tag{18}$$

and

$$OP_{V_1}^{dir, \infty} = 1 - (1 - \Omega_{\bar{f}_1} d_1^\alpha \chi) \sum_{s=0}^{m_{\bar{f}_1}-1} \frac{(\Omega_{\bar{f}_1} d_1^\alpha)^s \chi^s}{s!}. \tag{19}$$

3.2. Outage probability of V_2

Similarly, outage event occurs at V_2 and V_2 can successfully decode x_2 . Then, the outage performance of V_2 can be formulated as (20).

$$\begin{aligned} OP_{V_2} &= 1 - Pr(\Gamma_{R_2, x_2} \geq \varepsilon_2, \Gamma_{V_2, x_2} \geq \varepsilon_2) = 1 - Pr\left(|h_2|^2 \geq \frac{\varepsilon_2}{(\varphi_2 - \varepsilon_2\varphi_1)\rho}, |g_2|^2 \geq \frac{\varepsilon_2}{(\varphi_2 - \varepsilon_2\varphi_1)\rho}\right) = \\ &= 1 - \bar{F}_{|\bar{h}_2|^2}\left(\frac{\varepsilon_2 d_{BR_2}^\alpha}{\rho(\varphi_2 - \varepsilon_2\varphi_1)}\right) \bar{F}_{|\bar{g}_2|^2}\left(\frac{\varepsilon_2 d_{R_2 V_2}^\alpha}{\rho(\varphi_2 - \varepsilon_2\varphi_1)}\right). \end{aligned} \tag{20}$$

For further computation, OP_{V_2} is rewritten by (21).

$$OP_{V_2} = 1 - e^{-\frac{(\Omega_{\bar{h}_2} d_{BR_2} + \Omega_{\bar{g}_2} d_{R_2 V_2}) \varepsilon_2}{\rho(\varphi_2 - \varepsilon_2\varphi_1)}} \sum_{a=0}^{m_{\bar{h}_2}-1} \sum_{d=0}^{m_{\bar{g}_2}-1} \frac{1}{a! d!} \times (\Omega_{\bar{h}_2} d_{BR_2})^a (\Omega_{\bar{g}_2} d_{R_2 V_2})^d \left(\frac{\varepsilon_2}{\rho(\varphi_2 - \varepsilon_2\varphi_1)}\right)^{a+d}. \tag{21}$$

The outage probability of V_2 without UAV is expressed as (22).

$$\begin{aligned} OP_{V_2}^{dir} &= 1 - Pr(\bar{\Gamma}_{V_2, x_2}^{dir} > \varepsilon_2) = 1 - Pr\left(|f_2|^2 > \frac{\varepsilon_2}{\rho(\varphi_2 - \varphi_1 \varepsilon_2)}\right) = F_{|f_2|^2}\left(\frac{d_2^\alpha \varepsilon_2}{\rho(\varphi_2 - \varphi_1 \varepsilon_2)}\right) = \\ &= 1 - e^{-\frac{\Omega_{\bar{f}_2} d_2^\alpha \varepsilon_2}{\rho(\varphi_2 - \varphi_1 \varepsilon_2)}} \sum_{s=0}^{m_{\bar{f}_2}-1} \frac{(\Omega_{\bar{f}_2} d_2^\alpha \varepsilon_2)^s}{s! \rho^s (\varphi_2 - \varphi_1 \varepsilon_2)^s}. \end{aligned} \tag{22}$$

When $\rho \rightarrow \infty$, by using $e^{-x} \approx 1 - x$, and hence the asymptotic of $OP_{V_2}^\infty$ and $OP_{V_2}^{dir, \infty}$ are formulated by (23).

$$\begin{aligned} OP_{V_2}^\infty &= 1 - \left(1 - \frac{(\Omega_{\bar{h}_2} d_{BR_2} + \Omega_{\bar{g}_2} d_{R_2 V_2}) \varepsilon_2}{\rho(\varphi_2 - \varepsilon_2\varphi_1)}\right) \times \sum_{a=0}^{m_{\bar{h}_2}-1} \sum_{d=0}^{m_{\bar{g}_2}-1} \frac{(\Omega_{\bar{h}_2} d_{BR_2})^a (\Omega_{\bar{g}_2} d_{R_2 V_2})^d}{a! d!} \times \\ &\left(\frac{\varepsilon_2}{\rho(\varphi_2 - \varepsilon_2\varphi_1)}\right)^{a+d} \end{aligned} \tag{23}$$

and

$$OP_{V_2}^{dir, \infty} = 1 - \left(1 - \frac{\Omega_{\bar{f}_2} d_2^\alpha \varepsilon_2}{\rho(\varphi_2 - \varphi_1 \varepsilon_2)}\right) \times \sum_{s=0}^{m_{\bar{f}_2}-1} \frac{(\Omega_{\bar{f}_2} d_2^\alpha \varepsilon_2)^s}{s! \rho^s (\varphi_2 - \varphi_1 \varepsilon_2)^s}. \tag{24}$$

3.3. Ergodic capacity

3.3.1. Ergodic capacity of V_1

Since x_1 can be detected at the relay as well as at V_1 successfully, the achievable rate of x_1 is expressed by [31].

$$C_{x_1} = \frac{1}{2} \log(1 + \min(\Gamma_{R_1, x_1}, \Gamma_{V_1, x_1})). \quad (25)$$

Then, we obtain the ergodic capacity of x_1 as (26).

$$\bar{C}_{x_1} = \frac{1}{2} E\{\log(1 + \min(\Gamma_{R_1, x_1}, \Gamma_{V_1, x_1}))\} = \frac{1}{2 \ln 2} \int_0^\infty \frac{1 - F_X(x)}{1+x}, \quad (26)$$

where $X = \min(\Gamma_{R_1, x_1}, \Gamma_{V_1, x_1})$. Then, we can obtain the CDF of X as (27).

$$F_X(x) = 1 - e^{-\frac{(\Omega_{\bar{h}_1} d_{BR_1}^\alpha + \Omega_{\bar{h}_1} d_{R_1 V_1}^\alpha)}{\varphi_1 \rho} x} \times \sum_{s=0}^{m_{\bar{h}_1}-1} \sum_{b=0}^{m_{\bar{g}_1}-1} \frac{(\Omega_{\bar{h}_1} d_{BR_1}^\alpha)^s (\Omega_{\bar{g}_1} d_{R_1 V_1}^\alpha)^b x^{s+b}}{s! b! (\varphi_1 \rho)^{s+b}}. \quad (27)$$

Next, we express \bar{C}_{x_1} as (28).

$$\bar{C}_{x_1} = \frac{1}{2 \ln 2} \sum_{s=0}^{m_{\bar{h}_1}-1} \sum_{b=0}^{m_{\bar{g}_1}-1} \frac{(\Omega_{\bar{h}_1} d_{BR_1}^\alpha)^s (\Omega_{\bar{g}_1} d_{R_1 V_1}^\alpha)^b}{s! b! (\varphi_1 \rho)^{s+b}} \times \int_0^\infty \frac{x^{s+b+1} e^{-\frac{(\Omega_{\bar{h}_1} d_{BR_1}^\alpha + \Omega_{\bar{g}_1} d_{R_1 V_1}^\alpha)}{\varphi_1 \rho} x}}{1+x} dx. \quad (28)$$

With help [[32], (11)], we can rewrite as (29).

$$e^{-x} = G_{0,1}^{1,0} \left(x \middle| \begin{matrix} - \\ 0 \end{matrix} \right). \quad (29)$$

Based on [[33], (7.811.5)], \bar{C}_{x_1} is further computed by (30).

$$\bar{C}_{x_1} = \int_0^\infty \frac{x^{s+b}}{(1+x)} G_{0,1}^{1,0} \left(\frac{(\Omega_{\bar{h}_1} d_{BR_1}^\alpha + \Omega_{\bar{g}_1} d_{R_1 V_1}^\alpha)}{\varphi_1 \rho} x \middle| \begin{matrix} - \\ 0 \end{matrix} \right) dx = G_{1,2}^{2,1} \left(\frac{(\Omega_{\bar{h}_1} d_{BR_1}^\alpha + \Omega_{\bar{g}_1} d_{R_1 V_1}^\alpha)}{\varphi_1 \rho} \middle| \begin{matrix} -s-b \\ -s-b, 0 \end{matrix} \right). \quad (30)$$

Next, the ergodic rate of V_1 without UAV is given by (31).

$$\begin{aligned} \bar{C}_{x_1}^{dir} &= \frac{1}{2} E\{\log(1 + \bar{\Gamma}_{V_1, x_1}^{dir})\} = \frac{1}{2} E\{\log(1 + \varphi_1 \rho |f_1|^2)\} = \frac{1}{2 \ln 2} \int_0^\infty \frac{1}{1+x} [1 - F_{|f_1|^2} \left(\frac{d_1^\alpha x}{\varphi_1 \rho} \right)] dx = \\ &= \frac{1}{2 \ln 2} \sum_{s=0}^{m_{\bar{f}_1}-1} \frac{(\Omega_{\bar{f}_1} d_1^\alpha)^s}{s! (\varphi_1 \rho)^s} \int_0^\infty \frac{x^s e^{-\frac{\Omega_{\bar{f}_1} d_1^\alpha}{\varphi_1 \rho} x}}{1+x} dx \end{aligned} \quad (31)$$

Applying [[33], (3.353.5)] and some polynomial expansion manipulations, we can rewrite (31) as (32):

$$\bar{C}_{x_1}^{dir} = \frac{1}{2 \ln 2} \sum_{s=0}^{m_{\bar{f}_1}-1} \frac{(\Omega_{\bar{f}_1} d_1^\alpha)^s}{s! (\varphi_1 \rho)^s} \left[(-1)^{s-1} e^{-\frac{\Omega_{\bar{f}_1} d_1^\alpha}{\varphi_1 \rho}} \text{Ei} \left(-\frac{\Omega_{\bar{f}_1} d_1^\alpha}{\varphi_1 \rho} \right) + \sum_{k=1}^s (k-1)! (-1)^{s-k} \left(\frac{\Omega_{\bar{f}_1} d_1^\alpha}{\varphi_1 \rho} \right)^{-k} \right], \quad (32)$$

where $\text{Ei}(\cdot)$ is the exponential integral function.

3.3.2. Ergodic capacity of x_2

Similarly, we have achievable rate of V_2 as [31]:

$$C_{x_2} = \frac{1}{2} \log(1 + \min(\Gamma_{R_2, x_2}, \Gamma_{V_2, x_2})). \quad (33)$$

Then, the ergodic capacity is expressed by (34).

$$\bar{C}_{x_2} = \frac{1}{2} E\{\log(1 + \min(\Gamma_{R_2, x_2}, \Gamma_{V_2, x_2}))\} = \frac{1}{2 \ln 2} \int_0^\infty \frac{1 - F_Y(y)}{1+y} dy, \quad (34)$$

where $Y = \min(\Gamma_{R_2, x_2}, \Gamma_{V_2, x_2})$.

Then, we can obtain the CDF of X is

$$F_Y(y) = 1 - e^{-\frac{(\Omega_{\tilde{h}_2} d_{BR_2} + \Omega_{\tilde{g}_2} d_{R_2 V_2})}{\rho(\varphi_2 - x\varphi_1)} x} \sum_{a=0}^{m_{\tilde{h}_2}-1} \sum_{d=0}^{m_{\tilde{g}_2}-1} \frac{1}{a!d!} \times (\Omega_{\tilde{h}_2} d_{BR_2})^a (\Omega_{\tilde{g}_2} d_{R_2 V_2})^d \left(\frac{x}{\rho(\varphi_2 - x\varphi_1)}\right)^{a+d} \quad (35)$$

Next, \bar{C}_{x_2} is computed by (36).

$$\bar{C}_{x_2} = \frac{1}{2 \ln 2} \sum_{a=0}^{m_{\tilde{h}_2}-1} \sum_{d=0}^{m_{\tilde{g}_2}-1} \frac{(\Omega_{\tilde{h}_2} d_{BR_2})^a (\Omega_{\tilde{g}_2} d_{R_2 V_2})^d}{a!d!} \times \int_0^{\varphi_1} \left(\frac{y}{\rho(\varphi_2 - y\varphi_1)}\right)^{a+d} \frac{e^{-\frac{(\Omega_{\tilde{h}_2} d_{BR_2} + \Omega_{\tilde{g}_2} d_{R_2 V_2})}{\rho(\varphi_2 - x\varphi_1)} y}}{1+y} dy. \quad (36)$$

We continue to compute \bar{C}_{x_2} , then we have the new equation as in (37) at the top page. In which

$$\phi_n = \cos\left(\frac{2n-1}{2N} \pi\right) \text{ and } \Xi(x) = x \frac{\varphi_2}{2\varphi_1} + \frac{\varphi_2}{2\varphi_1}.$$

$$\begin{aligned} \bar{C}_{x_2} \approx & \frac{\varphi_2 \pi}{4\varphi_1 \ln 2N} \sum_{a=0}^{m_{\tilde{h}_2}-1} \sum_{d=0}^{m_{\tilde{g}_2}-1} \sum_{n=1}^N \left(\frac{\Xi(\phi_n)}{\rho(\varphi_2 - \Xi(\phi_n)\varphi_1)}\right)^{a+d} \frac{\sqrt{1 - \phi_n^2} (\Omega_{\tilde{h}_2} d_{BR_2})^a (\Omega_{\tilde{g}_2} d_{R_2 V_2})^d}{a!d!(1 + \Xi(\phi_n))} e^{-\frac{(\Omega_{\tilde{h}_2} d_{BR_2} + \Omega_{\tilde{g}_2} d_{R_2 V_2}) \Xi(\phi_n)}{\rho(\varphi_2 - \Xi(\phi_n)\varphi_1)}}. \end{aligned} \quad (37)$$

Finally, the ergodic rate of V_2 without UAV is given by (38).

$$\begin{aligned} \bar{C}_{x_2}^{dir} &= \frac{1}{2} E \left\{ \log \left(1 + \bar{\Gamma}_{V_2, x_2}^{dir} \right) \right\} = \frac{1}{2} E \left\{ \log \left(1 + \frac{\varphi_2 \rho |f_2|^2}{\varphi_1 \rho |f_2|^2 + 1} \right) \right\} = \\ &= \frac{1}{2 \ln 2} \int_0^{\varphi_1} \frac{1}{1+x} \left[1 - F_{|f_2|^2} \left(\frac{d_2^\alpha x}{\rho(\varphi_2 - \varphi_1 x)} \right) \right] dx. \end{aligned} \quad (38)$$

By the variable changing $q = \frac{x}{\varphi_2 - \varphi_1 x}$ and after few steps (38) can then

$$\begin{aligned} \bar{C}_{x_2}^{dir} &= \frac{1}{2 \ln 2} \int_0^\infty \left(\frac{1}{q + (\varphi_2 + \varphi_1)^{-1}} - \frac{1}{q + \varphi_1^{-1}} \right) \times \left[1 - F_{|f_2|^2} \left(\frac{d_2^\alpha q}{\rho} \right) \right] dq = \frac{1}{2 \ln 2} \sum_{s=0}^{m_{\tilde{f}_2}-1} \frac{(\Omega_{\tilde{f}_2} d_2^\alpha)^s}{s! \rho^s} \times \\ &= \int_0^\infty \left(\frac{1}{q + (\varphi_2 + \varphi_1)^{-1}} - \frac{1}{q + \varphi_1^{-1}} \right) \times q^s e^{-\frac{\Omega_{\tilde{f}_2} d_2^\alpha}{\rho} q} dq = \frac{1}{2 \ln 2} \sum_{s=0}^{m_{\tilde{f}_2}-1} \frac{(\Omega_{\tilde{f}_2} d_2^\alpha)^s}{s! \rho^s} \left[\frac{q^s e^{-\frac{\Omega_{\tilde{f}_2} d_2^\alpha}{\rho} q}}{q + (\varphi_2 + \varphi_1)^{-1}} - \frac{q^s e^{-\frac{\Omega_{\tilde{f}_2} d_2^\alpha}{\rho} q}}{q + \varphi_1^{-1}} \right] dq. \end{aligned} \quad (39)$$

We may rewrite (39) as follows by using [[33], (3.353.5)] and some polynomial expansion manipulations, the closed-form expression for the ergodic rate of V_2 without UAV is given by (40).

$$\begin{aligned} \bar{C}_{x_2}^{dir} &= \frac{1}{2 \ln 2} \sum_{s=0}^{m_{\tilde{f}_2}-1} \frac{\zeta^s}{s!} \left[\frac{q^s e^{-\zeta q}}{q + \beta_2} - \frac{q^s e^{-\zeta q}}{q + \beta_1} \right] dq = \\ &= \frac{1}{2 \ln 2} \sum_{s=0}^{m_{\tilde{f}_2}-1} \frac{\zeta^s}{s!} \left\{ [(-1)^{s-1} \beta_2^s e^{\beta_2 \zeta} \text{Ei}(-\beta_2 \zeta) + \sum_{k_1=1}^s (k_1 - 1)! (-\beta_2)^{s-k_1} \zeta^{-k_1}] - [(-1)^{s-1} \beta_1^s \times \right. \\ &\left. e^{\beta_1 \zeta} \text{Ei}(-\beta_1 \zeta) + \sum_{k_2=1}^s (k_2 - 1)! (-\beta_1)^{s-k_2} \zeta^{-k_2} \right\}. \end{aligned} \quad (40)$$

Remark 2: In the performance analysis, we achieve results with highly complicated parameters. Although it is very hard to evaluate which parameters play the main role in adjusting system performance, our analysis above has shown that different performance of two vehicles is still guaranteed by investigating specific parameters as in the next section.

3.4. Throughput analysis

Although OP plays an important role, another metric is also necessary to evaluate system performance, i.e., throughput in delay-limited transmission mode using UAV and without UAV is expressed by [[34], (24)].

$$\tau^{nodir} = (1 - OP_{V_1}) \bar{R}_1 + (1 - OP_{V_2}) \bar{R}_2, \text{ and } \tau^{dir} = (1 - OP_{V_1}^{dir}) \bar{R}_1 + (1 - OP_{V_2}^{dir}) \bar{R}_2. \quad (41)$$

4. NUMERICAL RESULTS

In this section, we perform Monte Carlo simulations to validate analytical results and analyze the performance of the proposed system model. Furthermore, to clearly compare the performance of the system, we also investigate my proposed scenario with the case of no UAV using the literature referred to [35]. We consider key metrics such as OP, EC, and throughput in the different configuration system parameters. The parameters used are summarized in Table 2, where BPCU is short for Bit per Channel use. Furthermore, it should be noted that normalized parameters have been established with $h = 1$ and $N = 20$.

Figure 2 depicts how $\bar{R}_1 = \bar{R}_2$ makes an influence on the performance of users V_1, V_2 . It can be seen that the performance of user V_1 is better than that of user V_2 . It is further confirmed that the performance of users following NOMA is better than that of users following OMA. In high SNR regions, SINR can be improved and then OP would be better. It is precisely seen that Monte-Carlo and analytical simulations are very well matched. In addition, the asymptotic curves match the exact curves. Two users exhibit different outage performance due to differences in power allocation to each user. Furthermore, a higher requirement of the target rate leads to a worse performance. It can be explained that the target rate limits the outage behavior in the expression to compute the outage (14) and (20). A comparison between NOMA, the research in [35], and situations without UAV are also shown in Figure 3.

Table 2. Table of parameters for numerical results

Parameters	Results
Monte Carlo simulation iterations	10^6
The power allocation coefficient	$\varphi_1 = 0.2, \varphi_2 = 0.8$
The target rate	$R_1 = R_2 = 1$ (BPCU)
The fading severity parameter	$m_{\bar{h}_1} = m_{\bar{h}_2} = m_{\bar{g}_1} = m_{\bar{g}_2} = m = 1$
The average power	$\lambda_{\bar{h}_1} = \lambda_{\bar{h}_2} = \lambda_{\bar{g}_1} = \lambda_{\bar{g}_2} = 1$
The path loss exponent	$\alpha = 2$

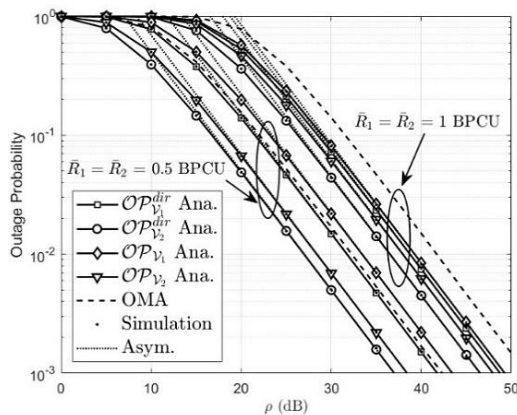


Figure 2. Outage probability versus SNR and varying $\bar{R}_1 = \bar{R}_2$

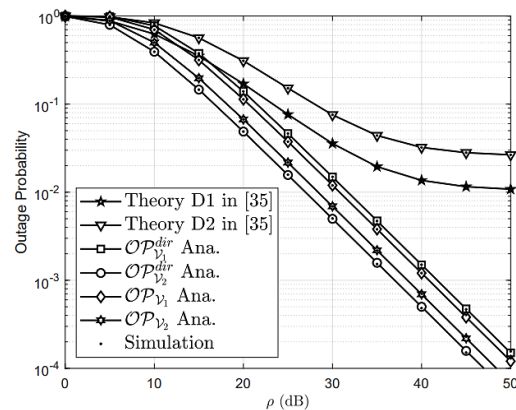


Figure 3. Outage probability versus SNR and with $m = 1, R_1 = R_2 = 0.5$ compare to [35]

Figure 4 shows the impact of UAV's height on outage performance. The superiority of user V_1 compared to user V_2 in terms of OP in Figure 2 remains only in low height, from 0 to 2.5. After this point, user V_2 exhibits its advantage in performance compared to the other user. The better channel condition of Nakagami- m fading brings to better performance, i.e., $m = 3$ is the case of best performance. Figure 5 illustrates the limitation of outage performance in high regions of the target rate that is related to factor $\varepsilon_1 = \varepsilon_2$. It is concluded that balance between demands for both target rate and OP keeps stable operation of such UAV networks. In this observation, $\rho = 30$ provides the superiority among two considered cases.

We can see the different ergodic capacity of two users in Figure 6. Such differences in terms of ergodic capacity can be clearly seen in the high SNR region. Interestingly, at higher SNR regions, the user's ergodic capacity V_1 can be significantly improved. In contrast, the ergodic capacity performance of user V_2 tends to be unchanged in the high SNR region. Figure 7 further provides the comparison between NOMA, the work in [35] and without the UAV. As observed in Figure 8, by varying the strength of channels, such ergodic capacity performance provides a similar trend reported in Figure 6.

We plot in Figure 9 the system throughput as a function of transmit SNR for various target rates. Depending on the outage probability, such throughput can be significantly improved in high SNR regions. The reason is that high SNR leads to lower outage probability and hence throughput approach to highest value. In this figure, throughput for the considered UAV network relying on NOMA is still better than that using OMA.

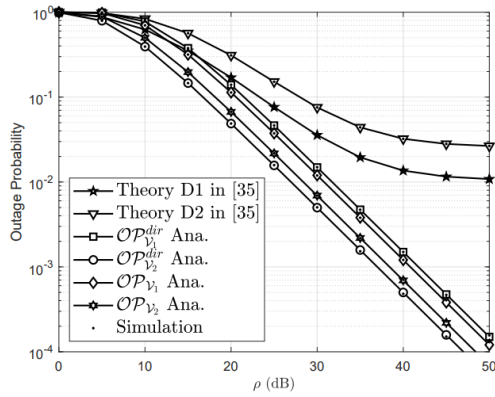


Figure 4. Ergodic capacity performance versus SNR and varying m

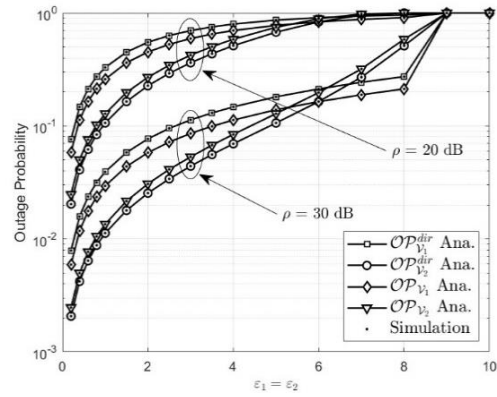


Figure 5. Outage probability versus SNR and varying $\bar{R}_1 = \bar{R}_2$

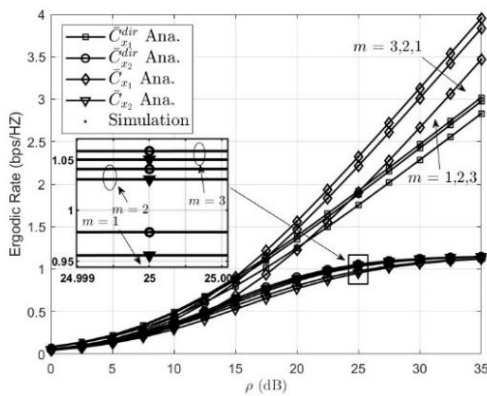


Figure 6. Ergodic capacity performance versus SNR and varying m

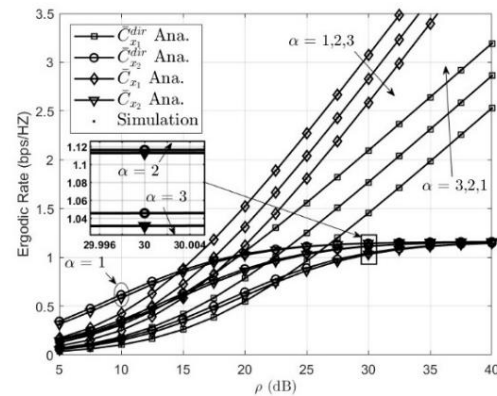


Figure 7. Ergodic capacity performance versus SNR and varying the path loss α

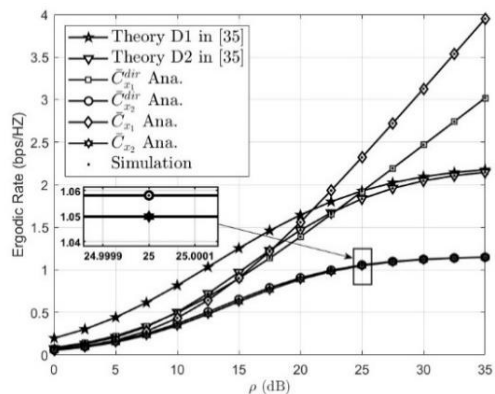


Figure 8. Ergodic capacity performance versus SNR with $m = 3, \varphi_1 = 0.2, \varphi_2 = 0.8$ compare to [35]

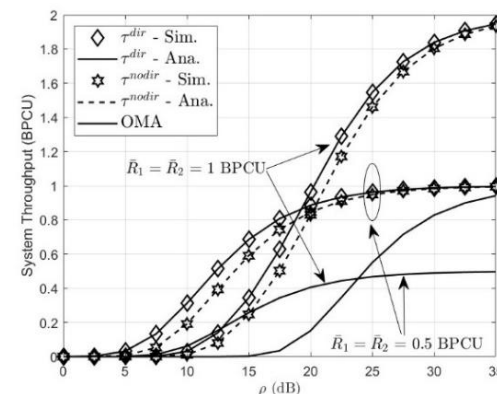


Figure 9. Throughput of the system versus SNR and varying $\bar{R}_1 = \bar{R}_2$

5. CONCLUSION

We have investigated an UAV-enabled half-duplex DF relaying system with joint design of NOMA and relaying protocol, subject to evaluation of outage and ergodic capacity. The design of the UAV relay results in improving serving areas. Based on the simulation results obtained, we show that user V1 is better than user V2 under specific conditions and parameters; thus, the NOMA scheme satisfies different demands for these users. Furthermore, we derived the exact closed-form expression of the outage probability and ergodic capacity to provide the guidelines to implement the proposed UAV mobile relay. However, the proposed UAV network is only applicable to single-pair and single-antenna users. In future work, we will consider the complex situation of multi-pairs and multi-antenna users.

ACKNOWLEDGEMENTS

The authors would like to thank the anonymous reviews for the helpful comments and suggestions. This work is a part of the basic science research program CSB2022-51 funded by the Saigon University.




REFERENCES

- [1] Y. Zeng, R. Zhang, and T. J. Lim, "Wireless communications with unmanned aerial vehicles: opportunities and challenges," *IEEE Communications Magazine*, vol. 54, no. 5, pp. 36–42, May 2016, doi: 10.1109/MCOM.2016.7470933.
- [2] M. Gharibi, R. Boutaba, and S. L. Waslander, "Internet of drones," *IEEE Access*, vol. 4, pp. 1148–1162, 2016, doi: 10.1109/ACCESS.2016.2537208.
- [3] P. H. Kopardekar, "Unmanned aerial system (UAS) traffic management (UTM): Enabling low-altitude airspace and UAS operations," *No. ARC-E-DAA-TN14211*, 2014.
- [4] S. D. Muruganathan *et al.*, "An overview of 3GPP release-15 study on enhanced LTE support for connected drones," *IEEE Communications Standards Magazine*, vol. 5, no. 4, pp. 140–146, Dec. 2021, doi: 10.1109/MCOMSTD.0001.1900021.
- [5] W. Mei and R. Zhang, "Cooperative downlink interference transmission and cancellation for cellular-connected UAV: A divide-and-conquer approach," *IEEE Transactions on Communications*, vol. 68, no. 2, pp. 1297–1311, Feb. 2020, doi: 10.1109/TCOMM.2019.2955953.
- [6] W. Mei, Q. Wu, and R. Zhang, "Cellular-connected UAV: Uplink association, power control and interference coordination," *IEEE Transactions on Wireless Communications*, vol. 18, no. 11, pp. 5380–5393, Nov. 2019, doi: 10.1109/TWC.2019.2936021.
- [7] J. Wang, C. Jiang, Z. Han, Y. Ren, R. G. Maunder, and L. Hanzo, "Taking drones to the next level: Cooperative distributed unmanned-aerial-vehicular networks for small and mini drones," *IEEE Vehicular Technology Magazine*, vol. 12, no. 3, pp. 73–82, Sep. 2017, doi: 10.1109/MVT.2016.2645481.
- [8] Y. Zeng, R. Zhang, and T. J. Lim, "Throughput maximization for UAV-enabled mobile relaying systems," *IEEE Transactions on Communications*, vol. 64, no. 12, pp. 4983–4996, Dec. 2016, doi: 10.1109/TCOMM.2016.2611512.
- [9] G. Sun, N. Li, X. Tao, and H. Wu, "Power allocation in UAV-enabled relaying systems for secure communications," *IEEE Access*, vol. 7, pp. 119009–119017, 2019, doi: 10.1109/ACCESS.2019.2932780.
- [10] R. Fan, J. Cui, S. Jin, K. Yang, and J. An, "Optimal node placement and resource allocation for UAV relaying network," *IEEE Communications Letters*, vol. 22, no. 4, pp. 808–811, Apr. 2018, doi: 10.1109/LCOMM.2018.2800737.
- [11] P. K. Sharma, D. Deepthi, and D. I. Kim, "Outage probability of 3-D mobile UAV relaying for hybrid satellite-terrestrial networks," *IEEE Communications Letters*, vol. 24, no. 2, pp. 418–422, Feb. 2020, doi: 10.1109/LCOMM.2019.2956526.
- [12] M. T. Mamaghani and Y. Hong, "On the performance of low-altitude UAV-enabled secure AF relaying with cooperative jamming and SWIPT," *IEEE Access*, vol. 7, pp. 153060–153073, 2019, doi: 10.1109/ACCESS.2019.2948384.
- [13] Y. Zeng, J. Xu, and R. Zhang, "Energy minimization for wireless communication with rotary-wing UAV," *IEEE Transactions on Wireless Communications*, vol. 18, no. 4, pp. 2329–2345, Apr. 2019, doi: 10.1109/TWC.2019.2902559.
- [14] T. Zhang, Y. Xu, J. Loo, D. Yang, and L. Xiao, "Joint computation and communication design for UAV-assisted mobile edge computing in IoT," *IEEE Transactions on Industrial Informatics*, vol. 16, no. 8, pp. 5505–5516, Aug. 2020, doi: 10.1109/TII.2019.2948406.
- [15] D. Yang, Q. Wu, Y. Zeng, and R. Zhang, "Energy tradeoff in ground-to-UAV communication via trajectory design," *IEEE Transactions on Vehicular Technology*, vol. 67, no. 7, pp. 6721–6726, Jul. 2018, doi: 10.1109/TVT.2018.2816244.
- [16] F. Tang, Z. M. Fadlullah, N. Kato, F. Ono, and R. Miura, "AC-POCA: Anti coordination game based partially overlapping channels assignment in combined UAV and D2D-based networks," *IEEE Transactions on Vehicular Technology*, vol. 67, no. 2, pp. 1672–1683, Feb. 2018, doi: 10.1109/TVT.2017.2753280.
- [17] D.-T. Do, "Optimal throughput under time power switching based relaying protocol in energy harvesting cooperative networks," *Wireless Personal Communications*, vol. 87, no. 2, pp. 551–564, Mar. 2016, doi: 10.1007/s11277-015-3120-9.
- [18] D.-T. Do, "Power switching protocol for two-way relaying network under hardware impairments," *Radio engineering*, vol. 24, no. 3, pp. 765–771, Sep. 2015, doi: 10.13164/re.2015.0765.
- [19] D.-T. Do and A.-T. Le, "NOMA based cognitive relaying: Transceiver hardware impairments, relay selection policies and outage performance comparison," *Computer Communications*, vol. 146, pp. 144–154, Oct. 2019, doi: 10.1016/j.comcom.2019.07.023.
- [20] Z. Ding *et al.*, "Application of non-orthogonal multiple access in LTE and 5G networks," *IEEE Communications Magazine*, vol. 55, no. 2, pp. 185–191, Feb. 2017, doi: 10.1109/MCOM.2017.1500657CM.
- [21] D.-T. Do, A.-T. Le, and B. M. Lee, "NOMA in cooperative underlay cognitive radio networks under imperfect SIC," *IEEE Access*, vol. 8, pp. 86180–86195, 2020, doi: 10.1109/ACCESS.2020.2992660.
- [22] D.-T. Do, T.-L. Nguyen, K. M. Rabie, X. Li, and B. M. Lee, "Throughput analysis of multipair two-way relaying networks with NOMA and imperfect CSI," *IEEE Access*, vol. 8, pp. 128942–128953, 2020, doi: 10.1109/ACCESS.2020.3008674.
- [23] W. Mei and R. Zhang, "Uplink cooperative NOMA for cellular-connected UAV," *IEEE Journal of Selected Topics in Signal Processing*, vol. 13, no. 3, pp. 644–656, Jun. 2019, doi: 10.1109/JSTSP.2019.2899208.
- [24] D. Hu, Q. Zhang, Q. Li, and J. Qin, "Joint position, decoding order, and power allocation optimization in UAV-based NOMA downlink communications," *IEEE Systems Journal*, vol. 14, no. 2, pp. 2949–2960, Jun. 2020, doi: 10.1109/STSP.2019.2899208.




- 10.1109/JSYST.2019.2940985.
- [25] N. Rupasinghe, Y. Yapici, I. Guvenc, and Y. Kakishima, "Non-orthogonal multiple access for mmWave drones with multi-antenna transmission," in *2017 51st Asilomar Conference on Signals, Systems, and Computers*, Oct. 2017, pp. 958–963, doi: 10.1109/ACSSC.2017.8335490.
- [26] G. Karagiannis *et al.*, "Vehicular networking: A survey and tutorial on requirements, architectures, challenges, standards and solutions," *IEEE Communications Surveys & Tutorials*, vol. 13, no. 4, pp. 584–616, 2011, doi: 10.1109/SURV.2011.061411.00019.
- [27] H. Yang, K. Zheng, K. Zhang, J. Mei, and Y. Qian, "Ultra-reliable and low-latency communications for connected vehicles: Challenges and solutions," *IEEE Network*, vol. 34, no. 3, pp. 92–100, May 2020, doi: 10.1109/MNET.011.1900242.
- [28] O. Abbasi, H. Yanikomeroglu, A. Ebrahimi, and N. M. Yamchi, "Trajectory design and power allocation for drone-assisted NRV2X network with dynamic NOMA/OMA," *IEEE Transactions on Wireless Communications*, vol. 19, no. 11, pp. 7153–7168, Nov. 2020, doi: 10.1109/TWC.2020.3008568.
- [29] D. Zhang, Y. Liu, L. Dai, A. K. Bashir, A. Nallanathan, and B. Shim, "Performance analysis of FD-NOMA-based decentralized V2X systems," *IEEE Transactions on Communications*, vol. 67, no. 7, pp. 5024–5036, Jul. 2019, doi: 10.1109/TCOMM.2019.2904499.
- [30] A. A. Khuwaja, Y. Chen, and G. Zheng, "Effect of user mobility and channel fading on the outage performance of UAV communications," *IEEE Wireless Communications Letters*, vol. 9, no. 3, pp. 367–370, Mar. 2020, doi: 10.1109/LWC.2019.2955444.
- [31] C. Guo, L. Zhao, C. Feng, Z. Ding, and H.-H. Chen, "Energy harvesting enabled NOMA systems with full-duplex relaying," *IEEE Transactions on Vehicular Technology*, vol. 68, no. 7, pp. 7179–7183, Jul. 2019, doi: 10.1109/TVT.2019.2914508.
- [32] V. S. Adamchik and O. I. Marichev, "The algorithm for calculating integrals of hypergeometric type functions and its realization in REDUCE system," in *Proceedings of the international symposium on Symbolic and algebraic computation*, Jul. 1990, pp. 212–224, doi: 10.1145/96877.96930.
- [33] I. S. Gradshteyn and I. M. Ryzhik, *Table of integrals, series, and products*. Amsterdam: Acad. Press, 2007.
- [34] X. Yue, Y. Liu, S. Kang, A. Nallanathan, and Z. Ding, "Exploiting full/half-duplex user relaying in NOMA systems," *IEEE Transactions on Communications*, vol. 66, no. 2, pp. 560–575, Feb. 2018, doi: 10.1109/TCOMM.2017.2749400.
- [35] B. C. Nguyen, T. M. Hoang, X. N. Pham, and P. T. Tran, "Performance analysis of energy harvesting-based full-duplex decode and forward vehicle-to-vehicle relay networks with nonorthogonal multiple access," *Wireless Communications and Mobile Computing*, vol. 2019, pp. 1–11, Nov. 2019, doi: 10.1155/2019/6097686.

BIOGRAPHIES OF AUTHORS






Hong-Nhu Nguyen    received a B.Sc. in electronics engineering from Ho Chi Minh City University of Technology in 1998 and an M.Sc. in electronics engineering from the University of Transport and Communications (Vietnam) in 2012. He is currently working as a lecturer at Saigon University, Ho Chi Minh City, Vietnam. He received a Ph.D. in communication technology from the Faculty of Electrical Engineering and Computer Science at VSB - Technical University of Ostrava, Czech Republic in 2021. His research interest includes applied electronics, wireless communications, cognitive radio, NOMA, and energy harvesting. He can be contacted via email: nhu.nh@sgu.edu.vn.



Nhat-Tien Nguyen    received the B.Eng. degree from the Posts and Telecommunications Institute of Technology and worked as a Senior Technician at Saigon Postal Corporation from 2003. He received the M.Eng. degree from the Ho Chi Minh City University of Technology (HCMUT) and received Ph.D. degree from the Technical University of Ostrava, Czech Republic, in 2017 and 2023, respectively. His research interests include MIMO, NOMA, D2D transmission, energy harvesting, millimeter wave communications, hybrid satellite-terrestrial networks, and wireless sensor networks. He can be contacted by email: tien.nn@sgu.edu.vn.



Gia-Thinh Vo    was born in Binh Duong Province, Vietnam. He received the B.S. and M.Sc. degrees from the Faculty of Electrical Engineering and Computer Science, Department of Electronics, at VSB-Technical University of Ostrava (VSB-TUO), Czech Republic, in 2019 and 2021, respectively. He is currently working as a lecturer at the Institute of Engineering - Technology at Thu Dau Mot University. Applied electronics, the internet of things, electrically controlled drives, and wireless communications are among his research interests. He can be contacted via email: thinhvg@tdmu.edu.vn.